Large-scale sensitivities of groundwater and surface water to groundwater withdrawal

Marc F.P. Bierkens[1,2,#], Edwin H. Sutanudjaja[1] and Niko Wanders[1]

[1]Department of Physical Geography, Utrecht University, P.O. Box 80115, 3508 TC Utrecht, The Netherlands
[2]Unit Soil and Groundwater Systems, Deltares, P.O. Box 85467, 3508 AL Utrecht, The Netherlands
Correspondence to: m.f.p.bierkens@uu.nl

Abstract

Increasing population, economic growth and changes in diet have dramatically increased the demand for food and water over the last decades. To meet increasing demands, irrigated agriculture has expanded into semi-arid areas with limited precipitation and surface water availability. This has greatly intensified the dependence of irrigated crops on groundwater withdrawal and caused a steady increase of groundwater withdrawal and groundwater depletion. One of the effects of groundwater pumping is the reduction in streamflow through capture of groundwater recharge, with detrimental effects on aquatic ecosystems. The degree to which groundwater withdrawal affects streamflow or groundwater storage depends on the nature of the groundwater-surface water interaction (GWSI). So far, analytical solutions that have been derived to calculate the impact of groundwater on streamflow depletion involve single wells and streams and do not allow the GWSI to shift from connected to disconnected, i.e. from a situation with two-way interaction to one with a one-way interaction between groundwater and surface water. Including this shift and also analyse the effects of many wells, requires numerical groundwater models that are expensive to setup. Here, we introduce an analytical framework based on a simple lumped conceptual model that allows to estimate to what extent groundwater withdrawal affects groundwater heads and streamflow at regional scales. It accounts for a shift in GWSI, calculates at which critical withdrawal rate such a shift is expected and when it is likely to occur after withdrawal commences. It also provides estimates of streamflow depletion and which part of the groundwater withdrawal comes out of groundwater storage and which parts from a reduction in streamflow. After a local sensitivity analysis, the framework is used to provide global maps of critical withdrawal rates and timing, the areas where current withdrawal exceeds critical limits, and maps of groundwater depletion and streamflow depletion rates that result from groundwater withdrawal. The resulting global depletion rates are compared with estimates from in situ-

38 observations, regional and global groundwater models and satellites. The analytical

39 framework is particularly useful for performing first-order sensitivity studies and for

40 supporting hydroeconomic models that require simple relationships between groundwater

41 withdrawal rates and the evolution of pumping costs and environmental externalities.

42

1. Introduction

44 Increasing population, economic growth and changes in diet have dramatically increased the

45 demand for food and water over the last decades (Godfray et al., 2010). To meet increasing

46 demands, irrigated agriculture has expanded into semi-arid areas with limited precipitation

47 and surface water (Siebert et al., 2015). This has greatly intensified the dependence of

48 irrigated crops on groundwater withdrawal (Wada et al., 2012) and caused a steady increase

49 of groundwater depletion rates (Wada and Bierkens, 2019). Recent estimates of current

50 groundwater withdrawal range approximately between 600-1000 km^3 yr^{-1} leading to

51 estimated depletion rates of 150-400 km^3 yr^{-1} (Wada, 2016).

52

53 Groundwater that is pumped comes either out of storage, from reduced groundwater

54 discharge or from reduction of evaporation fed from below by groundwater through capillary

55 rise and/or phreatophytes (Theis, 1940; Alley et al. 1999; Bredehoeft, 2002); Konikow and

56 Leake, 2014). Thus, extensive groundwater pumping not only leads to groundwater depletion

57 (Wada et al., 2010) but also to a reduction in streamflow (Wada et al., 2013; Mukherjee et al.,

58 2019; De Graaf et al., 2019; Jasechko et al., 2021) and desiccation of wetlands and

59 groundwater dependent terrestrial ecosystems (Runhaar et al 1997; Shafroth et al., 2000;

60 Elmore et al 2006; Yin et al 2018). However, the effect of groundwater pumping on

61 groundwater depletion and surface water depletion heavily depends on the nature of the

62 interaction between groundwater and surface water. Limiting ourselves to phreatic

63 groundwater systems and following Winter et al. (1998), a distinction can be made between

64 gaining streams, loosing streams and disconnected loosing streams, depending on the position

65 of the free groundwater surface with respect to the surface water level and the bottom of the

66 stream (Figure 1). Since groundwater pumping affects groundwater levels, it can move a

67 stream from gaining to losing to disconnected and loosing, which, in turn, affects the way

68 that groundwater pumping affects streamflow.
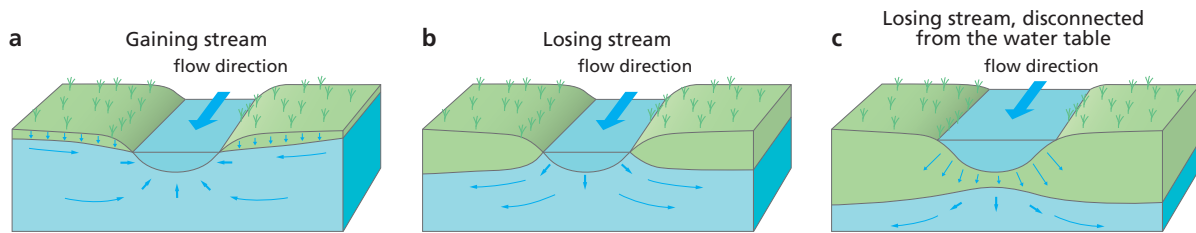
Fig. 1. Groundwater-streamflow interaction: (a) gaining stream; (b) losing stream; (c)losing stream disconnected from the water table; modified from Winter at al. (1998); credit to the United States Geological Survey.

Based on the above, Bierkens and Wada (2019) define two stages of groundwater withdrawal in phreatic aquifers. In stage 1, groundwater withdrawal is such that the water table remains connected with the surface water system (Figure 1a, b). Upon pumping, groundwater initially comes out of storage and groundwater levels decline. However, as groundwater levels decline around a well, the well attracts more of the recharge that would otherwise end up in the stream until a new equilibrium is reached where all of the pumped water comes out of captured streamflow. In a stage 1 withdrawal regime, withdrawal can be considered as physically stable, where groundwater depletion is limited and groundwater withdrawal mostly diminishes streamflow and evaporation. Depending on the groundwater level, one could further distinguish between gaining (Figure 1a) and loosing (Figure 1b) streams. This is important when considering the quality of pumped groundwater as in case of a losing stream surface water ends up in the well. In a stage 2 withdrawal regime, groundwater withdrawal is so large that groundwater levels fall below the bottom of the stream (Figure 1c). In that case, a further decline of the groundwater level hardly increases infiltration from the stream to the aquifer. Thus, in stage 2, groundwater withdrawal in excess of recharge and (constant) stream water infiltration is physically unstable and as a result leads to groundwater depletion and does not impact streamflow further if pumping rates increase.

From the above it follows that there is a critical transition between stage 1 and stage 2 groundwater withdrawal that depends on groundwater withdrawal rate. In reality, this transition is less abrupt. Right after the water table is just below the river bottom, negative pressure heads occur below the river bed while the soil is fully or partly saturated. Wang et al. (2015) show experimentally and theoretically that a full disconnection, i.e. the water table has no impact on the infiltration flux, occurs only when the depth of the groundwater table below the stream becomes larger than the stream water depth. Another reason is that these transitions does not occur abruptly is that multiple surface water bodies in the surroundings

100   of groundwater wells differ in depth depending on stream order and location in the river

101   basin. We also note that that in many regions of the world groundwater is pumped from

102   deeper confined or leaky-confined aquifers (De Graaf et al., 2017). Under confined

103   conditions, groundwaters-streamflow interaction only occurs for the larger rivers that are

104   deep enough to penetrate the confining layer, while in leaky confined aquifers the

105   interactions are more complicated and delayed (Hunt, 2003).

106

107   There are many analytical solutions for calculating the stream depletion rate (SDR), defined

108   as the ratio of the volumetric rate of water abstraction from a stream to groundwater pumping

109   rate. These solutions differ in assumptions about the type of aquifer (unconfined, confined,

110   leaky-confined, multiple aquifers), stream bottom elevation, stream geometry and including

111   additional resistance from the streambed clogging layer or not. We refer to Huang et al.

112   (2018) for an extensive overview of solutions and when to apply them. These analytical

113   solutions typically involve a single well and a single stream, or, using apportionment

114   methods, a single well and stream networks (Zipper et al., 2019), while they consider streams

115   to be connected with the water table. Such analytical solutions could possibly be used for

116   multiple wells using e.g. superposition. However, for more complex situations, with multiple

117   wells, increasing withdrawal rates and streams changing from e.g. connected to disconnected,

118   numerical groundwater models need to be used. These have the disadvantage that they are

119   parameter-greedy, time-consuming to setup and often computationally expensive. Thus,

120   relatively simple analytical tools to assess the effects of extensive multi-well groundwater

121   pumping on groundwater and surface water systems at large are lacking.

122

123   Here, we introduce a simple analytical framework based on a lumped conceptual model of

124   aquifer-stream interaction under pumping. The framework aims to describe at larger scales,

125   i.e. large catchments and/or regional-scale phreatic aquifer systems, to what extent multi-well

126   groundwater withdrawal affects area-average groundwater heads and streamflow. It allows

127   for a shift in the nature of groundwater-surface water interaction, calculates at which critical

128   withdrawal rate such a shift is expected and when it is likely to occur after withdrawal

129   commences. It also provides estimates of streamflow depletion and the partitioning between

130   groundwater storage depletion and reduction in streamflow (capture). We envision that such

131   an analytical framework is particularly useful for performing first-order sensitivity studies

132   and support hydroeconomic models that require simple relationships between large-scale

133 groundwater withdrawal rates and the evolution of pumping costs and environmental

134 externalities.

135

136 In the following, we first introduce the lumped conceptual model of large-scale groundwater

137 pumping with groundwater-surface water interaction. Next, we show its properties with an

138 extensive sensitivity analysis, followed with a global application of the model using inputs

139 and parameters from an existing global hydrological model (PCR-GLOBWB 2) and an

140 evaluation of its performance with estimates from in situ-observations, regional and global

141 groundwater models and satellites.

142
143

144 **2. Conceptual model of large-scale groundwater pumping with**

145 **groundwater-surface water interaction**

146
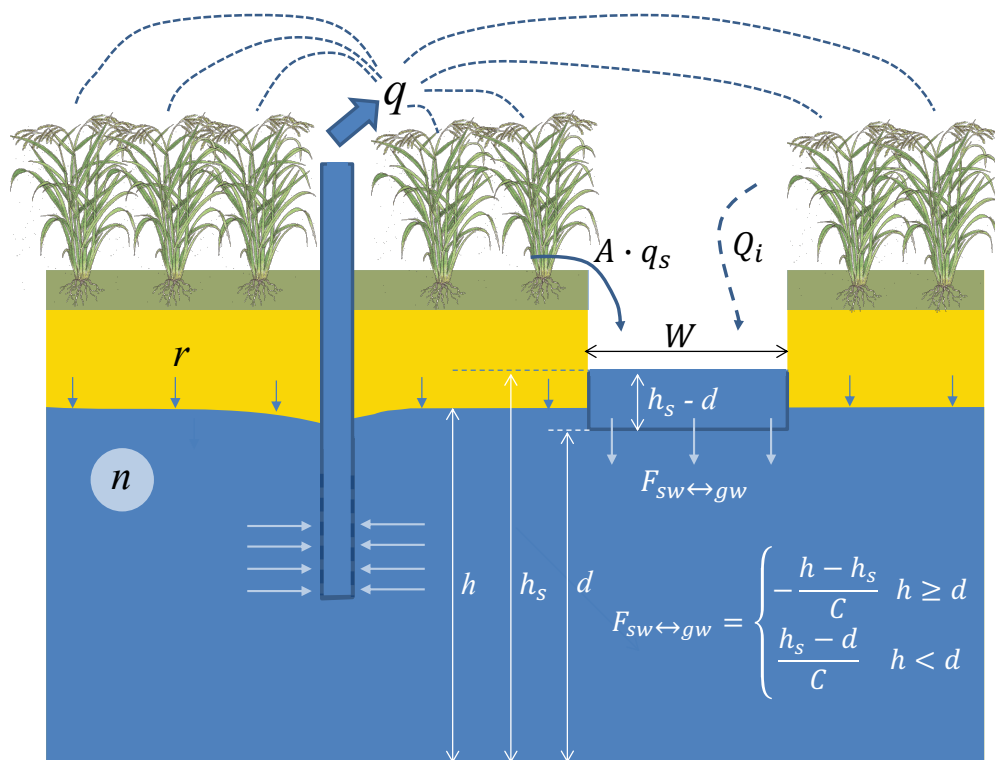
147
148 *Figure 2. Conceptual model of groundwater extracted (in this case for irrigation) from an*
149 *aquifer recharged by diffuse recharge and riverbed infiltration. Symbols are explained in the*
150 *text.*

151

152 A lumped conceptual hydrogeological model is proposed that allows for the analytical

153 treatment of area-average large-scale groundwater decline under varying pumping rates, yet

154 exhibits the properties of surface water-groundwater interaction. Consider a simplified model

155   of a phreatic aquifer subject to groundwater pumping (Figure 2). The volume of groundwater

156   pumped sums up all the pumping efforts of a large number of land owners that all draw water

157   from the same aquifer that can be seen as a common pool resource. Recharge consist of

158   diffuse recharge from precipitation and concentrated recharge from river-bed infiltration,

159   where river discharge comes from local surface runoff and from inflow from upstream areas

160   outside the area of interest.

161

162   Being of lumped nature, the model neglects (lateral) groundwater flow processes within the

163   aquifer and the mutual influence of multiple wells by treating the aquifer as one pool with a

164   given specific yield and unknown depth (i.e. physical limits are unknown) subject to pumping

165   treated as a diffuse sink. The latter is a simplification that represents the effects of hundreds

166   to thousands of wells of farmers spread more or less evenly across the aquifer. Also, we

167   assume withdrawal rate, surface runoff and river bed recharge to be constant in time,

168   neglecting seasonal variations that usually occur due to variation in crop water demand.

169   These simplifications allow us to represent the change of groundwater level h with a simple

170   linear differential equation of the total aquifer mass balance:

171

172    $$n\frac{dh}{dt} = r + F_{gw \leftrightarrow sw}(h) - q \tag{1}$$

173   With

174   h: groundwater head (m)

175   n: specific yield (-)

176   q: pumping rate per area ($m^3 \, m^{-2} \, y^{-1}$)

177    $F_{gw \leftrightarrow sw}$: surface water infiltration (or drainage) flux density ($m^3 \, m^{-2} \, y^{-1}$)

178

179   The groundwater - surface water flux is modelled as follows:

180    $$F_{gw \leftrightarrow sw}(h) = \begin{cases} -\frac{h - h_s}{C} & h \geq d \\ \frac{h_s - d}{C} & h < d \end{cases} \tag{2}$$

181   with h_s is the surface water level and d the elevation of the bottom of the water course. The

182   parameter C is a drainage resistance (days) which pools together all the parameters of

183   surface-water groundwater interaction, i.e. the density or area fraction of surface waters,

184   surface water geometry and river/lake-bed conductance and the hydraulic conductivity of the

185   aquifer. Equation (2) is also used to describe groundwater-surface water interaction in

186   numerical groundwater such as MODFLOW (McDonald and Harbaugh, 2005), as well as in

187 several large-scale hydrological models (Döll et al., 2014; Sutanudjaja et al., 2018). This is a

188 simplification of the true interaction where in case of a detachment of the groundwater level

189 and the river bed ($h < d$) negative pressure heads can occur below the river bed and Equation

190 (2) may underestimate the river bed infiltration (Brunner et al., 2010). However, this latter

191 study also shows that errors remain within 5% in case the surface water is deep enough (> 1

192 m). Equation (2) provides a critical transition in terms of the effect of pumping on the

193 hydrological system. As long as the groundwater level is above the bottom of the surface

194 water network, the groundwater-surface water flux acts as a negative feedback on

195 groundwater level decline, at the expense of surface water decline. As the water table falls

196 below the bottom elevation (only possible if pumping rate q is large enough; see hereafter),

197 surface water decline stops and progressive groundwater decline sets in.

198

199 The surface water level itself is a variable which is related to the surface water discharge Q

200 (m^3/day) and the groundwater level as follows:

201

202 $$Q = Wv(h_s - d) = Q_i + q_s A - F_{gw \leftrightarrow sw}(h)A \tag{3}$$

203 with

204 A: The area over the (sub-)aquifer considered (m^2)

205 q_s: surface runoff (m y^{-1})

206 Q_i: influx of surface water from upstream (m^3 y^{-1})

207 W: Stream width (m)

208 d: Bottom elevation stream (m)

209 v: Stream flow velocity (m y^{-1})

210

211 The influx Q_i is added to account for aquifers in dry climates where the surface water system

212 is fed by wetter upstream areas, e.g. mountain areas. The surface runoff q_s (including shallow

213 subsurface storm runoff) also supplements the streamflow. Equation (3) lumps the

214 streamflow system overlying the phreatic aquifer system with a representative discharge,

215 water height, flow velocity and stream width taken constant in time. Equations (1)-(3)

216 together describe the coupled surface water-groundwater system where all parameters and

217 inputs remain constant with time and groundwater head h and surface water levels h_s change

218 over time as a result of groundwater pumping only.

219

220   In Appendix A expressions are derived for the following properties of the coupled system:

221   q_{crit} Critical pumping rate (m^3 m^{-2} y^{-1}) above which the groundwater level becomes

222   disconnected from the stream.

223   t_{crit} Critical time (years after start of withdrawal) at which the groundwater level

224   becomes disconnected from the stream, i.e. $h < h_s$.

225    $h(t)$ Groundwater head (m) over time

226    $h(\infty)$ Equilibrium groundwater head (m) at $t=\infty$ that only occurs in case q $\leq q_{crit}$

227    $h_s(t)$ Surface water level (m) over time.

228    $h_s(\infty)$ Equilibrium surface water level (m), which is different when q $\leq q_{crit}$ than when

229   q $> q_{crit}$.

230    $Q(t)$ Surface water discharge (m^3 y^{-1}) over time.

231    $Q(\infty)$ Equilibrium surface water discharge (m^3 y^{-1}), which is different when q $\leq q_{crit}$

232   than when q $> q_{crit}$.

233    $q_{stor}(t)$ Part of the pumped groundwater that comes out of storage, which is different

234   when q $\leq q_{crit}$ than when q $> q_{crit}$.

235    $q_{cap}(t)$ Part of the pumped groundwater that comes from capture (reduction in

236   streamflow), which is different when q $\leq q_{crit}$ than when q $> q_{crit}$.

237

238   Table 1 provides an overview of the mathematical expressions derived for each of these

239   properties in Appendix A. The left column shows the stable regime where upon

240   commencement of pumping after some time an equilibrium is reached with equilibrium

241   groundwater levels $h(\infty)$, streamflow $Q(\infty)$ and surface water level h_s. The middle and right

242   columns show the results of unstable groundwater withdrawal. The behavior of $h(t)$, $Q(t)$ $h_s(t)$

243   follows that of the stable regime until time $t = t_{crit}$ when the groundwater level drops below

244   the bottom of the surface water. After this time the groundwater level $h(t)$ shows a persistent

245   decline and surface water level $h_s(t)$, streamflow $Q(t)$ and the fraction of water pumped from

246   capture become constant.

247

248

249

250

251

252

Table 1. Overview of derived expressions for groundwater properties used in this paper

$$\alpha = \frac{Q_i C + q_s AC + WvdC}{WvC + A} \qquad \beta = \frac{A}{WvC + A} \qquad q_{crit} = r + \frac{Q_i + q_s A}{WvC + A}$$

$q \leq q_{crit}$	$q > q_{crit}$	
	$t_{crit} = \dfrac{nC}{1-\beta} \ln\left(\dfrac{qC}{qC - (rC + \alpha) + d(1-\beta)}\right)$	
	$t \leq t_{crit}\ (h \geq d)$	$t > t_{crit}\ (h < d)$
$h(t) = \dfrac{rc+\alpha}{1-\beta} - \left(\dfrac{qC}{1-\beta}\right)\left[1 - e^{-\left(\frac{1-\beta}{nC}\right)t}\right]$ $h(\infty) = \dfrac{rc+\alpha-qC}{1-\beta}$	$h(t) = \dfrac{rc+\alpha}{1-\beta} - \left(\dfrac{qC}{1-\beta}\right)\left[1 - e^{-\left(\frac{1-\beta}{nC}\right)t}\right]$	$h(t) = d + \left[\dfrac{r-q}{n} + \dfrac{(Q_i + q_s A)}{n(WvC + A)}\right](t - t_{crit})$
$h_s(t) = \alpha + \beta h(t)$ $h_s(\infty) = \alpha + \dfrac{\beta(rc+\alpha-qC)}{1-\beta}$	$h_s(t) = \alpha + \beta h(t)$	$h_s = d + \dfrac{(Q_i + q_s A)C}{WvC + A}$
$Q(t) = Q_i + q_s A - \dfrac{A\alpha}{C} + \dfrac{A(1-\beta)}{C}h(t)$ $Q(\infty) = Q_i + (q_s + r - q)A$	$Q(t) = Q_i + q_s A - \dfrac{A\alpha}{C} + \dfrac{A(1-\beta)}{C}h(t)$	$Q = \dfrac{(Q_i + q_s A)WvC}{WvC + A}$
$q_{stor} = q e^{-\left(\frac{1-\beta}{nC}\right)t}$ $q_{cap} = q\left(1 - e^{-\left(\frac{1-\beta}{nC}\right)t}\right)$	$q_{stor} = q e^{-\left(\frac{1-\beta}{nC}\right)t}$ $q_{cap} = q\left(1 - e^{-\left(\frac{1-\beta}{nC}\right)t}\right)$	$q_{stor} = q - \left(r + \dfrac{(Q_i + q_s A)}{(WvC + A)}\right)$ $q_{cap} = r + \dfrac{(Q_i + q_s A)}{(WvC + A)}$

3. Local sensitivity analyses

Figure 3 shows the results of a sensitivity analysis for the critical withdrawal rate q_{crit} and the critical time until the water table disconnects from the stream t_{crit}. For the stable regime ($q \leq q_{crit}$) it shows the change in groundwater level at equilibrium $dh=h(0)-h(\infty)$, the change in streamflow at equilibrium $dQ = Q(0)-Q(\infty)$ and the e-folding time $t_{ef} = nC/(1-\beta)$ of reaching the equilibrium after the commencement of pumping. For the unstable regime, we show the decline rate of the groundwater level dh/dt, the (constant) streamflow depletion dQ and the constant fraction of capture ($f_{cap} = q_{cap}/q$). We stress that our sensitivity analysis is far from exhaustive (global) and that sensitivity plots are shown to provide a general feel of the behavior of the model and to show relationships between parameters and outputs that are of

266   interesting to show. Unless they are varied on one of the axes, the parameter values used are

267   the reference values denoted in Table 2.

268

269   *Table 2. Reference parameter values used in sensitivity analyses.*

Parameter	Value
Surface water system	
A	1000 km^2
q_s	0.001 m d^{-1}
Q_i	50 m^3 s^{-1}
d	95 m
W	20 m
v	1 m s^{-1}
Hydrogeology	
C	1000 d
n	0.3
r	0.001 m d^{-1}

270
271

272   Figure 3a shows that the critical withdrawal rate increases with the relative abundance of

273   surface water due to upstream inflow and runoff and decreases with a decreased strength of

274   the surface water-groundwater interaction (increased value of C). For stable withdrawal rates

275   we see the largest equilibrium groundwater level declines with increased pumping rates and

276   decreased strength of surface water-groundwater interaction, i.e. decreased capture (Figure

277   3c). Figure 3e shows that the equilibrium reduction in streamflow to be proportional to

278   groundwater withdrawal rate as expected, but to depend only mildly on the upstream inflow.

279   The latter is caused by the two-way interaction between surface water and groundwater:

280   increasing inflow for a given withdrawal rate reduces groundwater level decline, which in

281   turn limits the loss of surface water to the groundwater. As follows from the expression $t_{ef} =$

282   $nC/(1 - \beta)$, the time to equilibrium (Fig. 3g) , i.e. the time until the pumped groundwater

283   originates completely from capture and no further storge changes occur, is proportional to the

284   resistance value C and the specific yield, where the degree of proportionality depends on the

285   surface water properties. Figure 3g also shows that the time to full capture can be very large,

286   up to several decades.

287

288
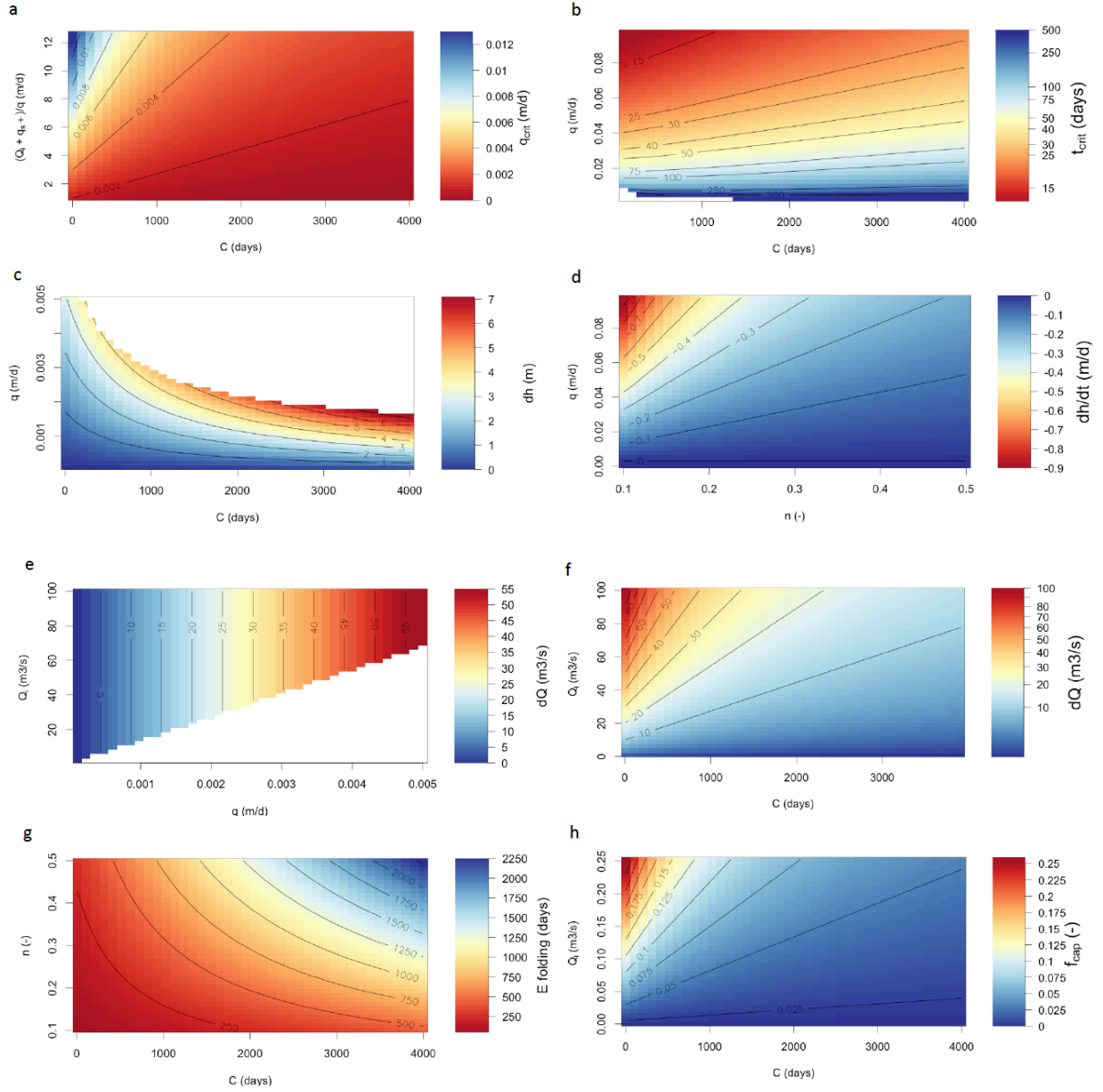
Figure 3. Results of the sensitivity analyses showing parameter dependence of q_{crit} (a) and
t_{crit} (b); variables under stable withdrawal: dh=h(0)-h(∞) (c), dQ=Q(0)-Q(∞) (e),
$t_{ef} = nC/(1 − β)$ (g)t_{crit} and variables under unstable withdrawal and t > t_{crit}: dh/dt (d), dQ
(f) and $f_{cap} = q_{cap}/q$.

Figures 3b-h (right column) provides sensitivity plots of relevant variables in the unstable

regime. Figure 3b shows that under the unstable regime, the time t_{crit} to a transition from a

connected to a non-connected groundwater table decreases with withdrawal rate, but slightly

increases with C. The latter seems counter-intuitive at first, because a larger value of C means

reduced surface water contribution and therefore likely larger groundwater level decline rates

and smaller values of t_{crit}. The equation for $h(t)$ in Table 1 (Equation A10 in the appendix)

shows that this is indeed the case for early times but that for later times the decline rates are

301 reduced by a larger value of C in the term factor $(1 - \beta)/nC$ in the exponential. Figures 3d-h

302 show sensitivity plots for $t > t_{crit}$ ($h < d$), i.e. groundwater levels are disconnected from the

303 surface water, groundwater is persistently taken out of storage and the capture becomes

304 constant. As expected, the groundwater level decline rates (Figure 3d) are proportional to

305 withdrawal rates and inversely proportional to specific yield. The final reduction in

306 streamflow (Figure 3f) for $t > t_{crit}$ decreases with the value of C (limited surface water-

307 groundwater interaction), while the availability of surface water is important for smaller

308 values of C. Here, a larger inflow leads to larger losses because losses are proportional to the

309 surface water level which increases with inflow. Figure 3h resembles that of Figure 3f

310 because apart from the constant recharge, the fraction of capture is proportional to the

311 streamflow reduction which ends up in the pumped groundwater

312

313

4. Global-scale application

315 *Global parameterization*

316 We applied the analytical framework to the global scale at 5 arc-minute resolution

317 (approximately 10 km at the equator) by obtaining parameters and inputs from the global

318 hydrology and water resources model PCR-GLOBWB 2 (Sutanudjaja et al., 2018, See Table

319 3 and Figures S1-S9 in the Supplement). For the flux densities q, q_s, r, the discharge Q_i and

320 the velocity v we used the average values over the period 2000-2015. Note that for an

321 application of the analytical framework at a cell-by-cell basis, the reduction in streamflow dQ

322 in a given cell should be accounted for by reducing the inflow Q_i to the downstream cell.

323 However, by using as inflow Q_i the upstream discharge from a PCR-GLOBWB simulation

324 that includes human water use, upstream withdrawals from surface water and groundwater

325 are already accounted for. Note that they would also be implicitly included in case an

326 observation-based streamflow dataset (e.g., Barbarossa et al., 2019) would have been used for

327 Q_i. The groundwater-surface water interaction parameter C is determined from the

328 characteristic response time J of the groundwater reservoir in PCR-GLOBWB 2, which is

329 based on the drainage theory of Kraijenhoff-van de Leur (1958). From this solution and

330 Equation (2) it can be shown that $C=J/n$ (see Appendix B). Since the variables q_{crit} and t_{crit}

331 depend heavily on the value of C we have also included the dataset of groundwater response

332 time published by Cuthbert et al. (2019) to calculate the C value.

333

334

335 *Table 3. Parameter and input values used in global-scale analyses at 5 arc-minute cells (~10*
336 *km ar the equator). All inputs obtained from PCR-GLOBWB 2 (Sutanudjaja et al., 2018),*
337 *except the C value obtained from PCR-GLOBWB and from Cuthbert et al. (2018); a input*
338 *variables averaged over the period 2000-2015.*

Parameter	Value
Surface water system	
A	Cell area 5 arc-minute cells (m^2)
q_s	Sum of surface runoff and interflow (m d^{-1}) of a cell
Q_i	Upstream discharge of a cell (m^3 d^{-1})
d	Stream elevation (m) based on bankfull discharge
W	Stream width (m) based on bankfull discharge
v	Calculated from bankfull discharge and stream depth (m d^{-1}) at Bankfull discharge, assuming v to be dependent on terrain slope only.
Hydrogeology	
C	$C = J/n$ (days), with J the characteristic response time of the groundwater reservoir (Sutanudjaja et al. 2018) or groundwater response times from Cuthbert et al. (2019).
n	Porosity values (-) from the groundwater reservoir in PCR-GLOBWB.
r	Net recharge (recharge minus capillary rise) (m d^{-1}).
q	Pumping rate (m d^{-1}).

339
340

Global results

342 Figure 4 shows the groundwater depletion rates q-q_{crit} for the areas with unstable

343 groundwater withdrawal. The resulting patterns are remarkably similar to those calculated

344 from previous global studies (Wada et al., 2012: Döll et al., 2014) and show the well-known

345 hotspots of the world. Total depletion rates in Figure 4 are 158 km^3 yr^{-1} (a) and 166 km^3 yr^{-1}

346 (b), which are in the range of previous studies, e.g., 234 km^3 yr^{-1} (Wada et al., 2012; year

347 2000), 171 km^3 yr^{-1} (Sutanudjaja et al., 2018; 2000-2015) and 113 km^3 yr^{-1} (Döll et al., 2014;

348 2000-2009).

349

350 The similarity of the groundwater depletion estimates with those obtained from global

351 hydrological models can be explained by the the fact that the way the groundwater-surface

352 water system is modelled in Figure 1 is similar to how the groundwater reservoirs and their

353 interaction with surface water have been implemented in global hydrological models such as

354 PCR-GLOBWB (De Graaf et al., 2015) and WGHM (Döll et al., 2014) (see also Appendix

355 B). Since the groundwater dynamics of latter models are (piece-wise) linear and groundwater

356 recharge in our model is applied directly in Equation (1) – i.e. the non-linear responses of the

357 soil system to precipitation and evaporation is bypassed -, forcing our model with average

fluxes r, q, Qi and q_s and using the parameter J from PCR-GLOBWB yields almost the same
depletion rates as from the time varying model simulations with PCR-GLOBWB. The small
difference between our estimate (158 km^3 yr^{-1}) and the value from PCR-GLOBWB 2
(Sutanudjaja et al., 2018) (171 km^3 yr^{-1}) is explained by a resulting non-linearity not
accounted for: during dry periods some of the streams in the PCR-GLOBWB run dry and do
not contribute to the concentrated recharge flux.
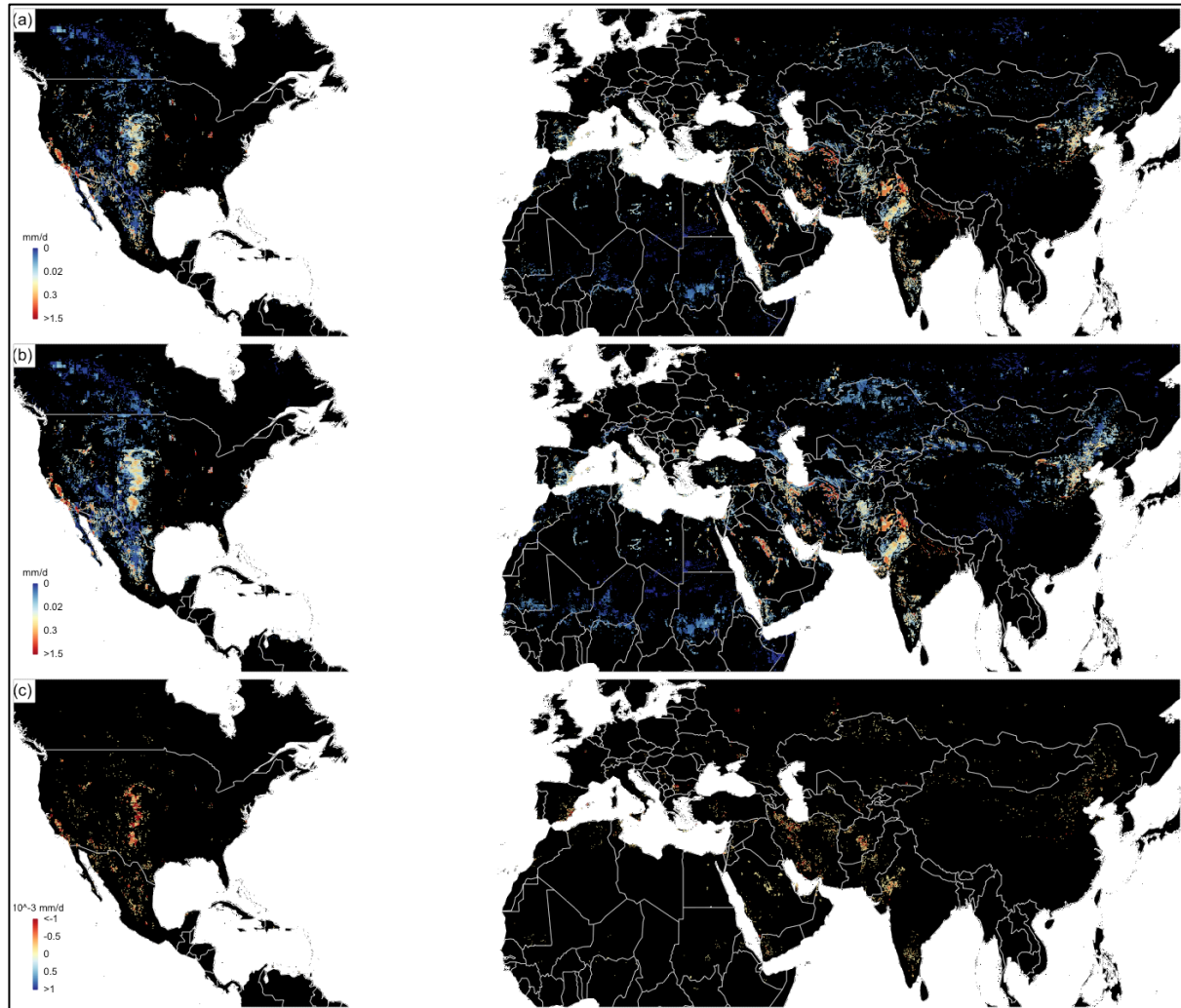
Figure 4. Average groundwater depletion rates (q-q_{crit}) over 2000-2015 at 5 arc-minute
resolution calculated with the data from Table 2. (a) using C-values from Sutanudjaja et al.
(2018); (b) using C-values based on Cuthbert et al. (2019); (c) difference map a – b.

Figure 5 shows the time to critical transition t_{crit} from both datasets. It is quite striking that,
although the depletion rates are rather similar between datasets (Figure 4), the critical
transition times are much larger for the Cuthbert et al. (2018) dataset, owing to its much
larger groundwater response times. Even though results are mildly sensitive to the value of C

374 (Figure 3b), the very large differences in response time between between these two datasets
375 also reveals that our method is only as good as its inputs.
376
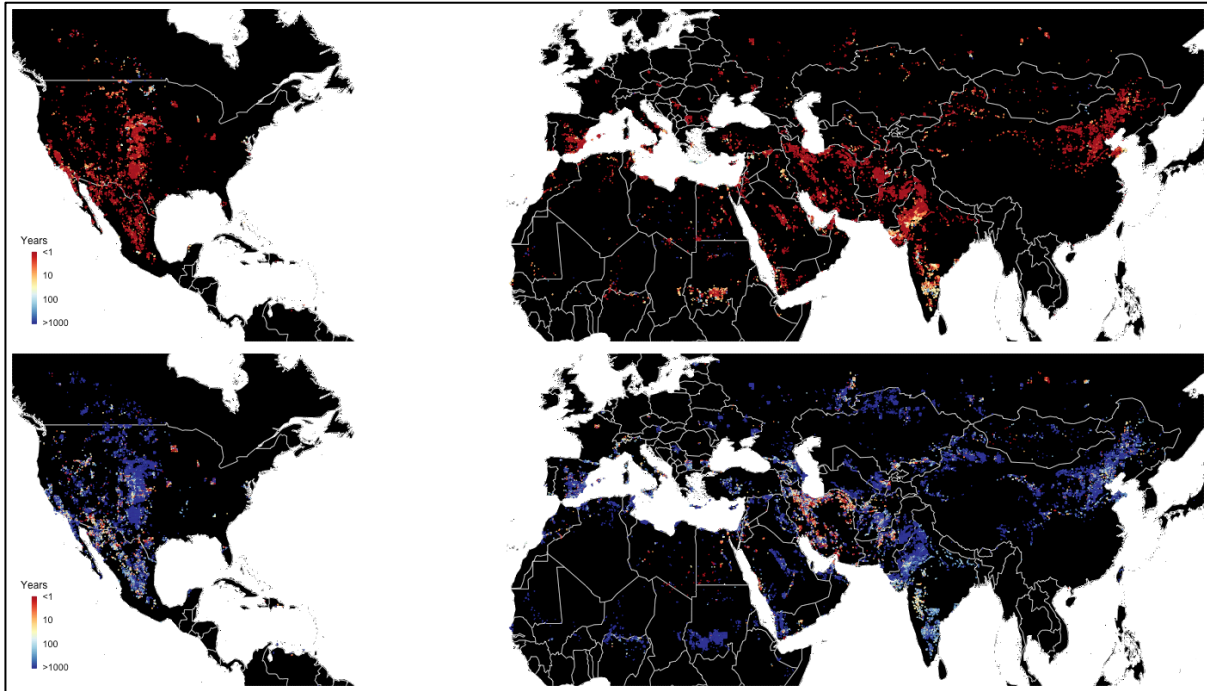
377
378 *Figure 5. Critical transition times (Critical time at which the groundwater level becomes*
379 *disconnected from the stream after start of pumping, i.e. $h < h_s$ in case $q > q_{crit}$) calculated*
380 *with the data from Table 1. The top figure uses C-values from Sutanudjaja et al. (2018) and*
381 *the lower figure from Cuthbert et al. (2019).*
382
383 To further explore the global impacts of groundwater withdrawal we calculated relevant
384 output variables for the areas that have been identified as subject to stable groundwater
385 withdrawal ($q \leq q_{crit}$; Figure 6) and unstable withdrawal ($q > q_{crit}$; Figure 7). Figure 6a
386 shows the equilibrium water table decline from stable groundwater withdrawal. We see the
387 largest declines occurring in areas with larger groundwater withdrawals, which are often
388 close to the depletion areas (Figure 4) and coincide with regions with limited surface water
389 occurrence due to a semi-arid climate (higher C-values). In contrast, the equilibrium decline
390 in streamflow (Figure 6b) is focused in areas with significant groundwater withdrawal and
391 higher surface water densities (low *C*-values), which are those areas that have a more semi-
392 humid climate where both groundwater and surface water use are present. These are also the
393 areas with relatively short times to equilibrium (Figure 6c).

394
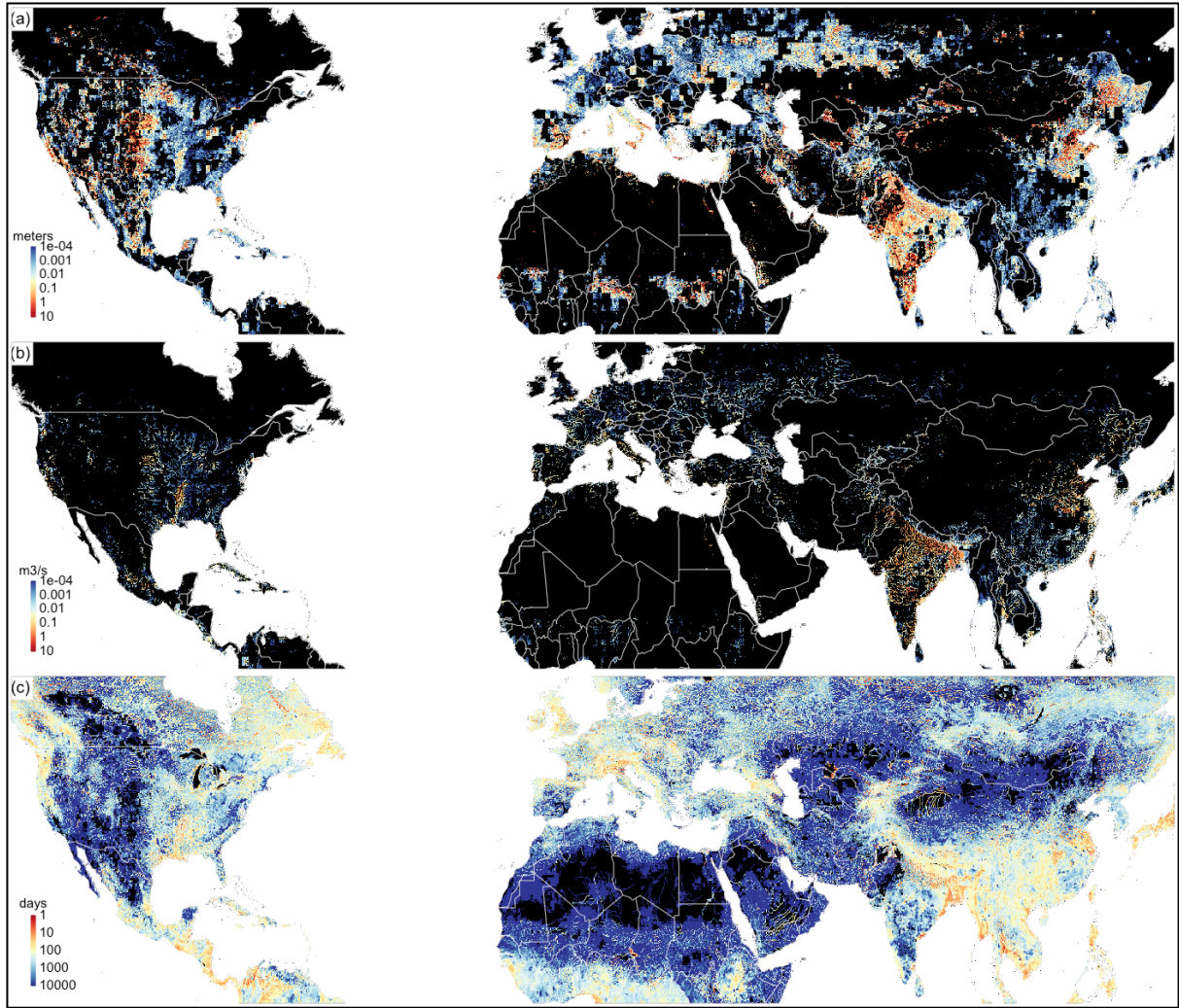
395 *Figure 6. Results for the areas with stable withdrawal rates (q $\leq q_{crit}$); (a) equilibrium*
396 *groundwater level decline (m); (b) equilibrium reduction of discharge ($m^3 s^{-1}$); (c) e-folding*
397 *time to complete capture (days); black areas are areas without groundwater withdrawal,*
398 *with unstable groundwater withdrawal or negligeable values.*

399

400 As expected, the groundwater decline rates under unstable withdrawal (Figure 7a) mirror the

401 depletion rates (Figure 4). Estimates based on piezometers for major depleting areas are in

402 the order of 0.4-1.0 m yr^{-1} in Southern California and the Southern High Plains aquifer

403 (Scanlon et al., 2012) and 0.1-1.0 m yr^{-1} in the Gangetic plain (MacDonald et al., 2016). Our

404 estimates are in the lower end of those observed ranges, which could be partly explained by

405 the fact that, particularly in the U.S., groundwater withdrawal is from semi-confined aquifers,

406 leading to a larger head decline per volume out of storage than follows from the specific

407 yields used in our conceptual model. The largest change in streamflow and the highest

408 fraction of capture are found in areas where groundwater depletion coincides with the

409 presence of surface water, e.g. such as the Northern and Eastern part of the Ogallala aquifer,

410 the Indus basin and southern India.

411
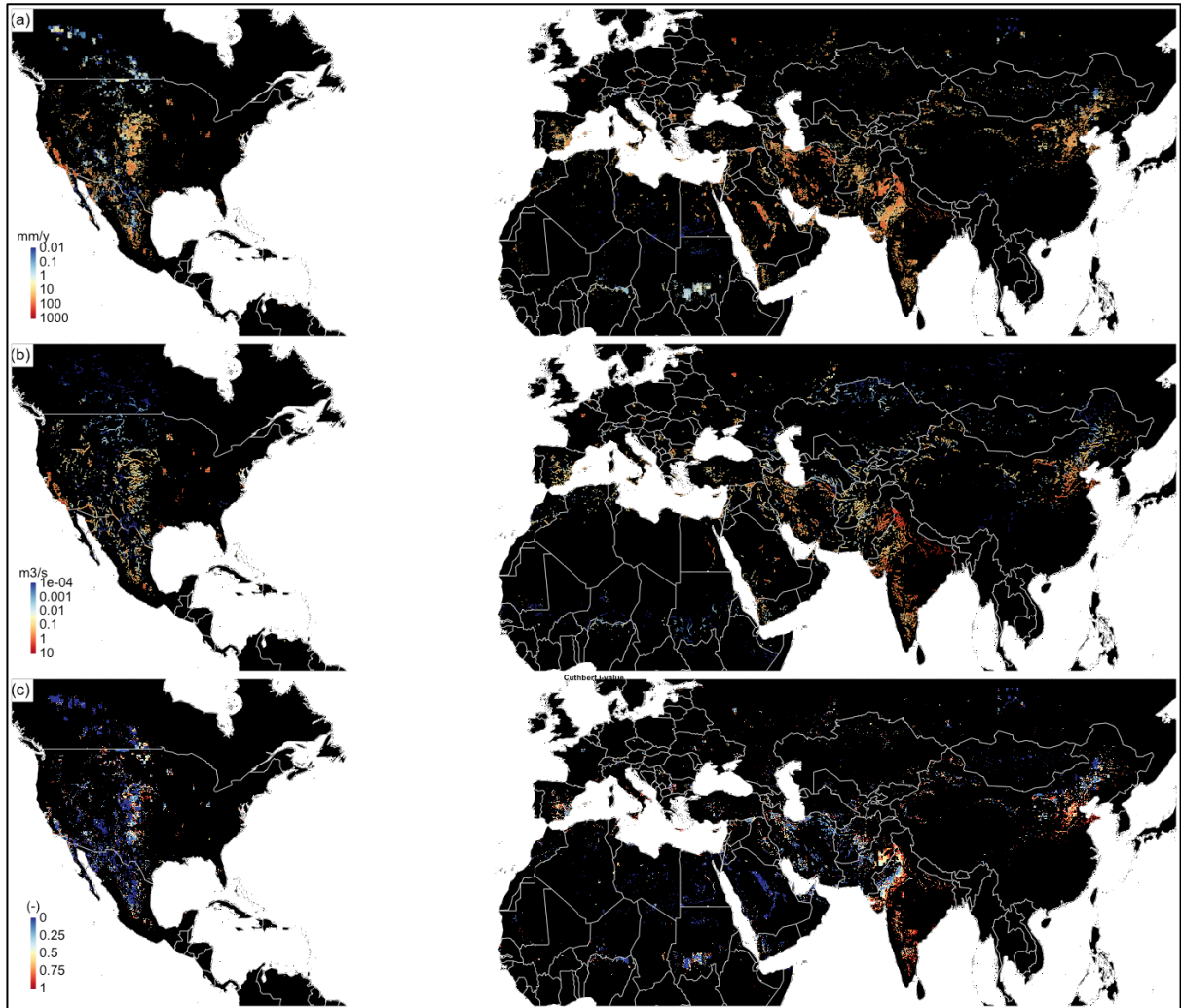
Figure 7. Results for the areas with unstable withdrawal rates ($q > q_{crit}$); (a) groundwater
level decline rate (mm yr^{-1}); (b) equilibrium reduction of discharge (m^3 s^{-1}); (c) fraction of
capture (-); black areas are areas without groundwater withdrawal, with stable groundwater
withdrawal or with negligeable values.

Sensitivity and evaluation of global results

Critical parameters that determine the stream-aquifer interaction and hence many of the
outputs shown in Figures 4-7 are the stream-aquifer resistance parameter C and the stream
bottom elevation d. We performed a local sensitivity analysis by changing the parameters C
and d ±10% around their current values (Figures S3 and S6 in Supplement) and calculated the
relative change in the output per unit relative change in parameters C and d. The results
(Supplementary Table S1) reveil that for most outputs the sensitivity to C and d is limited
(below unity). A notable exception is the sensitivity of t_{crit} to d which can be quite large,
particularly for the lower values of C from Sutanudjaja et al. (2018). From the sensitivity
analysis we conclude that the global results are relatively robust to changes in the parameters

428 *C* and *d*, except for the critical time to stream-aquifer disconnection which is sensitive to *d*
429 and to a lesser extend to *C*.

430

431 To evaluate our global results we compare these with observations and model results at
432 various scales, working from large to smaller scales (both in extent and resolution). These
433 include: aquifer average storage change from the Gravity Recovery and Climate Experiment
434 (GRACE) satellite, global-scale groundwater and streamflow depletion estimates from a
435 global groundwater model (De Graaf et al., 2019), continental-scale (conterminous U.S.)
436 groundwater and streamflow depletion estimates from Parflow-CLM (Condon and Maxwell,
437 2019) and groundwater flow and streamflow decline rates for the Republican River Basin
438 based on in-situ observations (Wen and Chen, 2006; McGuire, 2017).

439

440 From the results in Figure 4a (with *C* from Sutanudjaja et al., 2018; assuming $q > q_{crit}$ and
441 $t > t_{crit}$) we computed average depletion rates of the world's major aquifers subject to
442 depletion (following Richey et al., 2015) and compared these with average trends in total
443 water storage (TWS) from GRACE (Gravity Recovery and Climate Experiment) gravity
444 anomalies over the period 2003-2015 (Figure 8). We used the JPL GRACE Mascon product
445 RL05M (Wiese, 2015; Watkins et al., 2015; Wiese et al., 2016). We did not correct TWS for
446 changes in other hydrological stores, assuming the latter to be approximately constant over a
447 13-year period in semi-arid areas with limited surface water and TWS trends to mainly reflect
448 groundwater depletion. Figure 8 shows that the estimated depletion rates are reasonably
449 consistent with the GRACE estimates, particularly for the known hotspot aquifers with the
450 largest depletion. Notable exceptions are an overestimation of the depletion rate in the Paris
451 Basin and underestimation of depletion rates of the Maranhao Basin, the North Caucasus
452 Basin and the North African Aquifer Systems. These differences may be caused by errors in
453 withdrawal data from PCR-GLOBWB 2 (Supplementary Figure S9), errors in streamflow
454 leakage and errors that result from not correcting the GRACE products for possible secular
455 trends in other hydrological stores. A notable effect could be that by assuming aquifers to be
456 unconfined, we overestimate the leakage from surface water to groundwater in pumped
457 confined aquifers, leading to an underestimation of depletion rates. It should also be noted
458 however that the aquifers whose depletion rates are underestimated have estimated GRACE
459 trends between 1-10 mm/year, just above the accuracy limit of GRACE TWS trends (viz.
460 Richey et al., 2015).
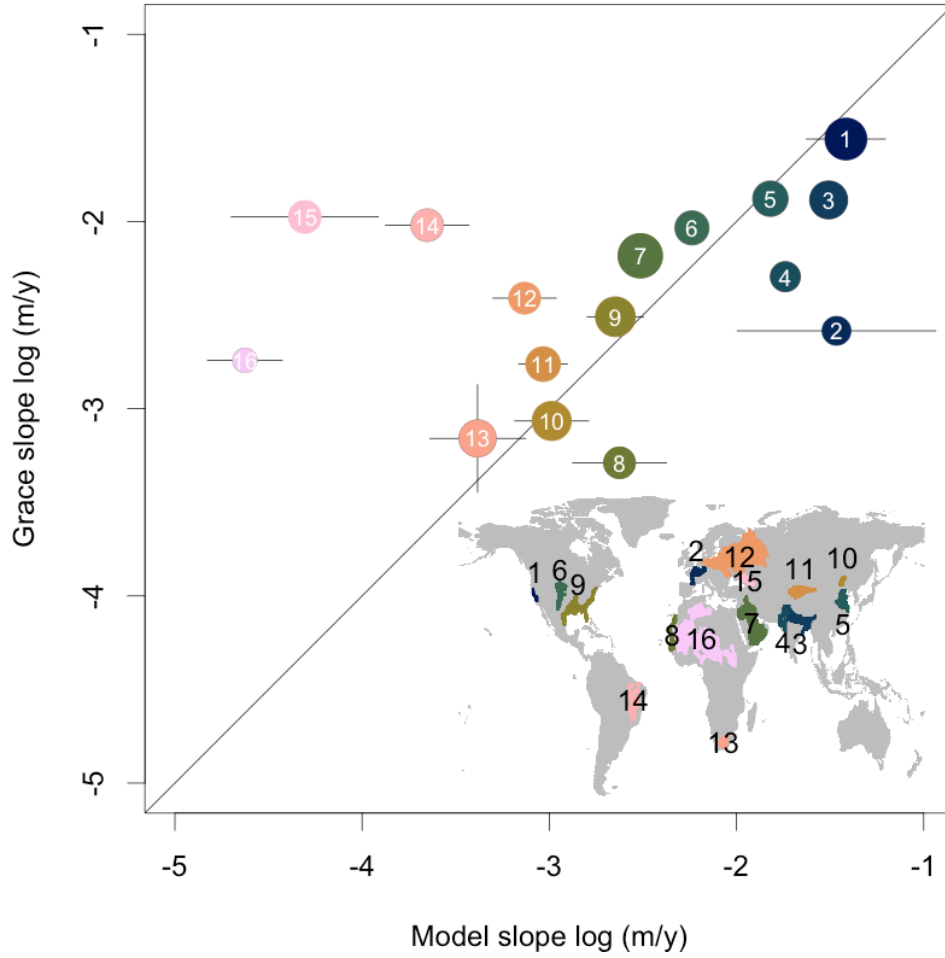
461
462
463 *Figure 8. Comparison of depletion rates in Figure 4a for major groundwater basins with*
464 *average depletion rates from GRACE (m yr^{-1}). Size of the circles is proportional to aquifer*
465 *area; crosses are standard errors in estimated mean aquifer trends; 1: Central Valley*
466 *(California); 2: Paris Basin; 3 Ganges-Brahmaputra Basin; 4; Indus Basin; 5: North China*
467 *Plane; 6. Ogallala (High Plains) Aquifer; 7. Arabian Aquifer System; 8: Senegalo-*
468 *Mauretanian Basin; 9: Atlantic and Gulf Coastal Plains Aquifer; 10: Song-Liao Basin; 11:*
469 *Tarim basin; 12; Russian Platform Basins; 13: Karoo Bason; 14: Maranhao Basin; 15:*
470 *North Caucasus Basin; 16: North African Aquifer Systems.*
471
472 At the global scale, we compared the head decline rate (mm d^{-1}) calculated with the analytical
473 framework with average decline rates over the period 2000-2015 as obtained from the global
474 groundwater model of De Graaf et al (2019). Note that we restricted this comparison to the
475 areas with unstable withdrawal rates ($q > q_{crit}$, $t > t_{crit}$). The results shown in Figure S10 show
476 that the patterns of high and low values of the two estimates are similar, but that the
477 estimated decline rates from our analytical framework are larger than those estimated by De
478 Graaf et al. (2019). The most likely cause for the larger values in our approach is that it
479 neglects the impact of lateral flow (accross cell boundaries) or that the *J*-value of PCR-

480   GLOBWB used to calculate the C parameter (see Appendix B) is too large so that leakage

481   from the streams is underestimated. Comparison of the stream depletion estimates from the

482   analytical framework (See Supplement Fig. S11; assuming $q > q_{crit}, t > t_{crit}$ or $q < q_{crit}, t >> t_{ef}$)

483   shows similar patterns to that of De Graaf et al. (2019), but also slightly larger values. Thus,

484   the most likely cause for the larger depletion values of our analytical framework (Figure S10)

485   is the neglect of lateral flow between cells.

486

487   At the continental scale, we compared groundwater storage changes (m) and stream depletion

488   (% of mean annual flow) across part of the conterminous U.S. obtained from a ParFlow-CLM

489   model (Condon and Maxwell, 2019) with the global estimates from our analytical

490   framework. ParFlow simulates coupled groundwater and surface water flow by solving the

491   3D Richards' equation and the diffusive wave equation respectively, while the community

492   land model CLM includes land surface processes such as evaporation, plant water use, snow

493   accumulation and snow melt. Condon and Maxwell (2019) calculate the total effects of

494   pumping from the predevelopment stage (1900 until 2008), while our global results are based

495   on the average withdrawal rates for the period 2000-2015. To make our results comparable

496   with those of Condon and Maxwell (2019), we took their reported total storage loss of ~1000

497   km^3 since 1900 and determined the period length for which the total groundwater withdrawn

498   based on Sutanudjaja et al (2018) across the U.S. approximately equals 1000 km^3. This

499   resulted in the period 1965-2015. We subsequently recalculated the global maps using the

500   average groundwater withdrawal rate over 1965-2015 from Sutanudjaja et al. (2018).

501   The results are shown in the Supplementary Figures S12 (for $q > q_{crit}, t > t_{crit}$) and S13

502   ($q > q_{crit}, t > t_{crit}$ or $q < q_{crit}, t >> t_{ef}$). Figure S12 shows again that the analytical approach

503   yields larger depletion estimates than ParFlow, but the results are more similar than with de

504   global model of De Graaf et al (2019).

505

506   Figure S13 (top) shows the percentage reduction of streamflow by groundwater pumping

507   since predevelopment as calculated by ParfFlow-CLM and Figure S13 (bottom) the

508   estimates based on the analytical framework. We show both maps for reference in the

509   Supplement, but it turns out that comparing the streamflow reduction of the analytical

510   framework with that of ParfFlow-CLM is inhibited by differences in model output and

511   presentation. The ParfFlow-CLM results represent cumulative dQ as fraction of Q, whereas

512   the results from the analytical framework represent marginal dQ as a fraction of Q, which

513   makes the results only comparable for the headwater catchments. Also, the difficulty of

514 comparison due to the resolution gap (ParfFlow-CLM: 1 km; analytical framework: 5

515 arcminutes ~ 10 km) is exacerbated due to the different map formats (vector and vs. raster).

516 Therefore, we refrain from further comments and show the maps as they are.

517

518 At the basin scale, we compared our global results with trends in groundwater head decline

519 and streamflow decline as obtained from observations of groundwater levels and surface

520 water discharge in the Republican River Basin (U.S.A.). The Republican Basin runs through

521 the northern part of the High Plains Aquifer system which is heavily influenced by

522 groundwater withdrawal. We used data from a study by Wen and Chen (2006) that estimated

523 trends in streamflow over the period 1950-2003 for 24 gauging stations spread across the

524 Republican river and its tributuaries. The trends were adjusted for possible trends in

525 precipitation and are therefore assumed to only reflect a decrease in streamflow as a result of

526 groundwater pumping. This resulted in 18 out of the 24 stations with significant negative

527 trends. Wen and Chen (2006) also provide groundwater level observations from three wells

528 with filters in the Ogallala formation at three location positioned in three representative

529 locations in the Republican Basin. We used the analytical framework with global parameters

530 (Table 3) but with the average values of q, q_s, r, Q_i over the period 1960-2003 obtained from

531 PCR-GLOBWB (Sutatudjaja et al., 2009) to estimate at 5 arcminute resolution average

532 groundwater level decline rates (m/year). Figure S14 in the Supplement shows box plots of

533 streamflow trends and groundwater head trends from the observations and from our

534 framework. The distribution of estimated streamflow decline overlaps with that from the

535 observed trends with a slight underestimation. The observed groundwater head decline rates

536 however are underestimated. This may be caused by the fact that we only have three

537 observations which are from a mostly confined aquifer where small storage coefficients lead

538 to larger decline rates.

539

540 To further investigate the performance of our method in reproducing groundwater level

541 declines at the sub-basin scale, we compare estimated groundwater level declines between

542 2002-2015 from 1522 groundwater wells in the Republican Basin obtained from McGuire,

543 (2017). Figure S15 shows maps and boxplots of observed groundwater level declines (m) and

544 declines estimated from the analytical framework. Although the overall pattern of

545 groundwater depletion in the Republican Basin is reproduced, there are occasional outlieres

546 in the global estimates that are not seen in the observations. This is likely the result from the

547 global withdrawal data that are obtained by downscaling the total US groundwater

withdrawal to 5-arcminutes based on 5-arcminute estimates of total groundwater demand (Sutanudjaja et al., 2018). Although these downscaled withdrawal rates are well verified at the county-scale (See Wada et al, 2012), the mismatch at the 5-arcminute scale can be large. Thus, when using global datasets, the analytical framework is limited to the sub-basin scale and too coarse for local-scale estimates. Improvements can be expected when local data on groundwater withdrawal are available at finer resolution.

Critical limits to groundwater withdrawal for major basins

We finish the result section by summarizing critical limits to groundwater withdrawal for the major river basins of the world. In Figure 9a the median value of q_{crit} is plotted for the major basins in the world (sub-watershed level of HydroBasins, Lehner et al., 2008) together with the areas where groundwater withdrawal is on average unstable over the years 2000-2015. This figure provides, at first order, a global map of the maximum limit to physically stable groundwater withdrawal rates. The parts of the world where the critical withdrawal rates are very small largely coincide with the band of countries that experience high values of water stress (Hofsté et al., 2019). This shows that there is little room in these areas to supplement water demand without causing groundwater depletion.
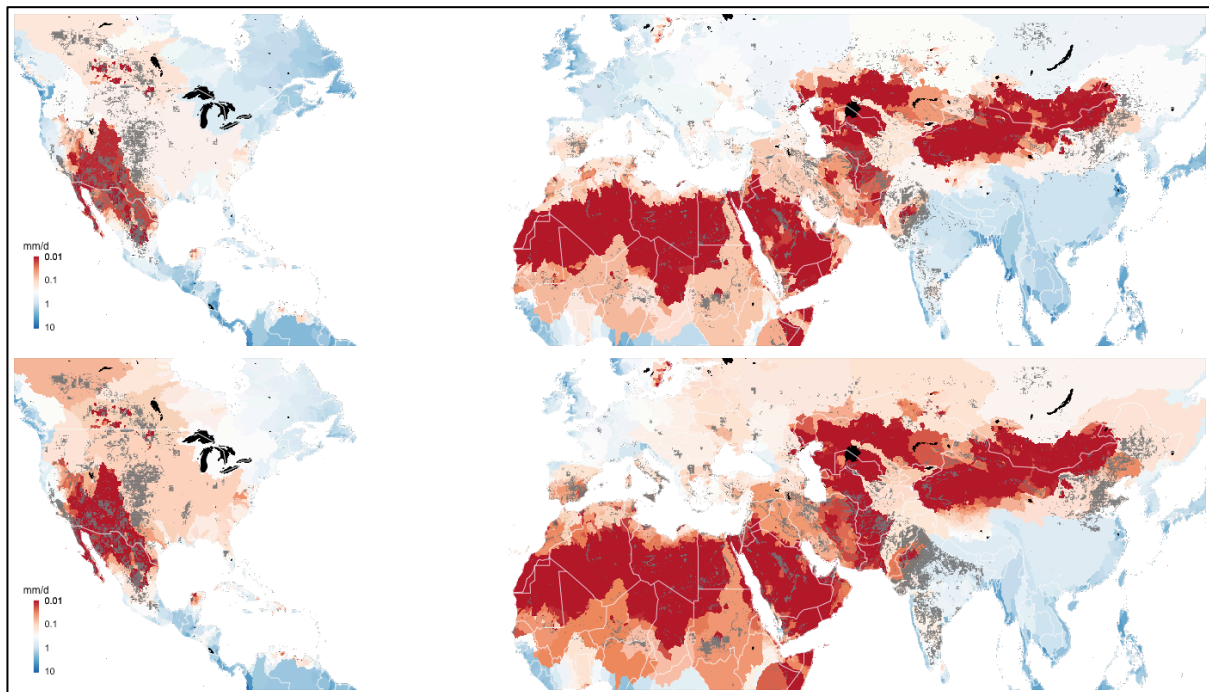
Figure 9. Global limits to stable groundwater withdrawal rate; top: limit to physically stable groundwater withdrawal mapped as the median q_{crit} per sub-basin (based on Hydro-basins: Lehner et al., 2008), grey-shaded areas are those for which $q>q_{crit}$; bottom: limit to ecologically stable groundwater withdrawal mapped as the median q_{eco} per sub-basin, grey-shaded areas are those $q>q_{eco}$.

571 The ecological limits to groundwater withdrawal, q_{eco}, can be defined as the withdrawal rate

572 that is low enough to prevent streamflow from dropping below some environmental flow

573 limit Q_{env}, i.e. a value that is high enough to safeguard the integrity of the aquatic ecosystems

574 (Linnansaari et al. 2013; Pastor et al 2014). The value of q_{eco} can be calculated by inverting

575 Equation (A14) and taking $Q(\infty) < Q_{env}$:

576 $$q_{eco} = \frac{(Q_i + (q_s + r)A) - Q_{env}}{A} \qquad (4)$$

577 We note that environmental flows are usually defined during low flow conditions (Pastor et

578 al 2014; Gleeson and Richter, 2018), so it may be more appropriate to use the value of $Q(\infty)$

579 as the average over the summer half year instead of yearly averages. If we assume that the

580 average streamflow regime follows a cosine function with a period of 1 year, then the

581 average (natural) streamflow Q_s in summer would be equal to:

582 $$Q_s = \left(1 - \frac{2}{\pi}\right)[(Q_i + (q_s + r)A] \qquad (5)$$

583 and q_{eco} becomes:

584 $$q_{eco} = \frac{\left(1 - \frac{2}{\pi}\right)[Q_i + (q_s + r)A] - Q_{env}}{A} \qquad (5)$$

585 In Figure 9 (bottom) we have plotted q_{eco} using, as an example, Q_{env} to be 20% of the

586 average natural summer streamflow Q_s. The resulting map can be seen as a first order

587 approximation of the limits to ecologically stable groundwater withdrawal. In most cases,

588 $q_{eco} < q_{crit}$ as is also evident from the larger grey-shaded areas in the bottom figure compared

589 to the top figure. The results suggest that supplementing water demand by groundwater use in

590 the world's water stressed areas is limited under ecological constraints. We stress that the

591 sub-basin scale critical and environmental limits are meant for large-scale environmental

592 assessment, not for local groundwater management.

593

594 **4. Discussion and conclusions**

595

596 We have introduced an analytical framework based on a lumped conceptual model that

597 intents to describe to what extent groundwater withdrawal affects groundwater heads and

598 streamflow under changing regimes of groundwater-surface water interaction. Despite its

599 simplicity, the framework is able to provide a rich tableau of hydrologically, economically

600 and ecologically relevant outputs, produces results at the global scale that are similar to those

601 obtained with global hydrological models, with the advantage of a significant reduction in

602 data and computational requirements.

603

604   The estimated global groundwater and surface water depletion rates were compared with

605   observations and model results at various scales (support and extent), with mixed but overall

606   favourable results up to the sub-basin scale. We stress that output variables that are related to

607   critical environmental limits such as q_{crit}, q_{eco}, t_{crit} and t_{ef} are difficult to validate directly,

608   particularly at the larger scales at which our framework operates. This would require large-

609   scale pumping experiments or metering of pumping wells in basins while surface water and

610   groundwater are intensively monitored over decades. As such, the critical limits are non-

611   observables calculated with a model that is only partly validated with a limited set of output

612   variables, i.e. groundwater level decline and streamflow depletion. We note however that this

613   limitation is not restricted to our analytical framework, but occurs for any analytical or

614   numerical groundwater model used.

615

616   Our analytical framework can be used in GIS-based scoping studies to provide first-order

617   estimates of the regional-scale impact of future groundwater pumping on groundwater levels,

618   or to approximate regional-scale ecological or physical limits to groundwater pumping.

619   Another possible application is in hydroeconomic modelling, where the equations in Table 1

620   can be used as regionally varying hydrological response functions (Harou et al., 2009;

621   MacEwan et al., 2017) in hydroeconomic optimization – where model evaluations need to be

622   fast - in order to infer socially optimal pumping rates that include environmental externalities.

623

624   Clearly, many complicating factors are neglected in our approach, e.g.: underground spatial

625   heterogeneity, including the occurrence of multiple aquifer systems and semi-confined layers

626   that are present in many important alluvial groundwater basins; the variable depth and

627   topology of the surface water system and the intermittent nature of many streams in semi-arid

628   to semi-humid areas; and the locations of the wells with respect to the streams. Of these, the

629   neglect of confining layers may be one of the more crucial limitations of the approach. For

630   instance, a considerable part of the groundwater used for irrigation in the big alluvial basins

631   of the U.S. (e.g. Ogallala and Central Valley of California), where farmers have the financial

632   resources to drill deep wells (Perrone and Jasechko, 2019), is pumped from deeper confined

633   aquifers. This means that the groundwater-surface water interaction is limited to the large

634   rivers and lakes only and that head decline per volume water pumped is larger than in

635   phreatic conditions. It would in principle be possible to include the effect of a confining layer

636   by using a larger value of the groundwater-surface water resistance parameter C, a smaller

637   value of recharge r and a storage coefficient instead of specific yield. Similarly, the impacts

638   of seasonably variable boundary conditions of q, q_s and Q_i could be taken into account by

639   simple convolution, considering that the groundwater level responses $h(t)$ and dh/dt (Table 1)

640   are respectively step and impulse responses of a linear system. Also, the effects of multiple

641   streams with variable stream bottom elevations could be included by extending the piecewise

642   linearization of Equation (2) to more domains (e.g. Bierkens and te Stroet, 2007). However,

643   we argue that such extensions are not in the spirit of the simple analytical framework

644   developed, which intents to provide first order sensitivies at larger scales. If the addition of

645   complexity is needed to provide more accurate assessments for a specific case, it would be

646   more logical to build a tailor-made numerical groundwater flow model.

647

648   We end with the note that a global application of our conceptual analytical framework is not

649   restricted to the use of data from the PCR-GLOBWB repository. The necessary fluxes r, q, Q_i

650   and q_s can also be obtained from other repositories of multi-model re-analyses such as

651   EartH2Observe (Schellekens et al., 2017) and from the combination of remotely sensed

652   estimates of hydrological variables (Lettenmaier et al., 2015; McCabe et al., 2017), e.g.

653   estimating recharge and surface runoff from remotely sensed precipitation, evaporation and

654   soil moisture change, and using high-resolution global datasets on discharge (Barbarossa et

655   al., 2018) and river bed dimensions (Allen and Pavelsky, 2018; Lehner et al., 2018).

Data availability.

The data used in the global assessments provided by PCR-GLOBWB 2 can downloaded
from: https://doi.org/10.4121/uuid:e3ead32c-0c7d-4762-a781-744dbdd9a94b. The
groundwater response times of Cuthbert et al. (2019) can be found on:
https://doi.org/10.6084/m9.figshare.7393304 GRACE data used for validation are obtained
from: https://doi.org/10.5067/TEMSC-OCL05. The Republican River Basin well data from
2002-2015 can be downloaded from https://pubs.er.usgs.gov/publication/sim3373.

Author contributions.

MB conceived and designed the study. NW and MB performed the calculations. NW and
EHS performed the model validation. MB wrote the paper. All authors read, commented on,
and revised the manuscript.

Competing interests.

The authors declare that they have no conflict of interest.

Acknowledgements.

Niko Wanders acknowledges funding from NWO 016.Veni.181.049. The comments and
suggestions by the Editor, reviewer Grant Ferguson and two anonymous reviewers
significantly improved the manuscript.

References

676 **References**

678 Allen, H. and Pavelsky, M. (2018). Global extent of rivers and streams. *Science* 361, 585-
679   588.
680 Alley, W.M., Reilly, T. E. and Franke, O. L. (1999). Sustainability of groundwater resources
681   *United States Geological Survey Circular* 1186.
682 Barbarossa, V., Huijbregts, M., Beusen, A. *et al.* (2018). FLO1K, global maps of mean,
683   maximum and minimum annual streamflow at 1 km resolution from 1960 through
684   2015. *Sci Data* 5, 180052.
685 Bierkens, M.F.P. and Te Stroet, C.B.M (2007). Modelling non-linear water table dynamics
686   and specific discharge through landscape analysis. *J. Hydrol.* 332, 412– 426.
687 Bierkens, M.F.P. and Wada, Y. (2019). Non-renewable groundwater use and groundwater
688   depletion: a review. *Environ. Res. Lett.* 14 063002.
689 Condon, L.E. and Maxwell, R.M. (2019). Simulating the sensitivity of evapotranspiration and
690   streamflow to large-scale groundwater depletion. *Sci. Adv*. 5, eaav4574.
691 Cuthbert, M.O., Gleeson, T., Moosdorf, N. *et al.* (2019). Global patterns and dynamics of
692   climate–groundwater interactions. *Nature Clim. Change* 9, 137–141.
693 de Graaf, I.E.M., van Beek, L.P.H., Wada, Y., and Bierkens, M.F.P. (2014). Dynamic
694   attribution of global water demand to surface water and groundwater resources: Effects of
695   abstractions and return flows on river discharges, *Adv. Water Resour*. 64, 21–33.
696 de Graaf, I.E.M., Gleeson, T., van Beek, L.P.H., Sutanudjaja, E.H. and Bierkens, M.F.P.
697   (2019). Environmental flow limits to global groundwater pumping. *Nature* 574, 90-108.
698 Döll, P., Müller Schmied, H., Schuh, C., Portmann, F.T. and Eicker, A. (2014), Global-scale
699   assessment of groundwater depletion and related groundwater abstractions: Combining
700   hydrological modeling with information from well observations and GRACE satellites.
701   *Water Resour. Res*. 50, 5698–5720.
702 Elmore, A.J., Manning, S.J., Mustar, J.F. and Craine J.M. (2006). Decline in alkali meadow
703   vegetation cover in California: the effect of groundwater extraction and drought. *J. Appl.*
704   *Ecol.* 43, 770–9.
705 Gleeson, T., Moosdorf, N., Hartmann, J., and van Beek, L. P. H. (2014). A glimpse beneath
706   earth's surface: GLobal HYdrogeology MaPS (GLHYMPS) of permeability and porosity,
707   *Geophys. Res. Lett*., 41, 3891–3898
708 Gleeson, T. and Richter, B. (2018). How much groundwater can we pump and protect
709   environmental flows through time? Presumptive standards for conjunctive management of
710   aquifers and rivers. *River Res. Appl*. 34 83–92.
711 Godfray, H.C.J., Beddington, J.R, Crute, I.R., Haddad, L., Lawrence, D., Muir, J.F. et al.
712   (2010). Food security: The challenge of feeding 9 billion people. *Science* 327, 812–818.
713 Harou, J.J., Pulido-Velazquez, M., Rosenberg, D.E., Medellín-Azuara, J., Lund, J. R. and
714   Howitt, R. E. (2009). Hydro-economic models: concepts, design, applications, and future
715   prospects. *J. Hydrol*. 375 627–43.
716 Hofste, R.W.,Kuzma, S., Walker, S., Sutanudjaja, E.H., Bierkens, M.F.P., Kujiper, M.J.M.,
717   Sanchez, M.F., van Beek, R., Wada, Y., Rodríguez, S.G. (2019). *Aqueduct 3.0: Updated*
718   *Decision-Relevant Global Water Risk Indicators*; Technical Note World Resources
719   Institute, Washington, DC, USA, 2019; https://www.wri.org/publication/aqueduct-30

720

721 Huang, S.-H., Yang, T. and Yeh, H.-D. (2018). Review of analytical models to stream
722   depletion induced by pumping: Guide to model selection. *J. Hydrol* 561, 277-285.
723 Hunt, B., 2003. Unsteady stream depletion when pumping from semiconfined aquifer. *J.*
724   *Hydrol. Eng.-ASCE* 8, 12–19.
725 Jasechko, S., Seybold, H., Perrone, D., Fan, Y. and Kirchner, J. (2021). Widespread potential
726   loss of streamflow into underlying aquifers across the USA. *Nature* 591, 391–395.
727 Konikow, L.F. and Leake, S.A. (2014). Depletion and capture: Revisiting "the source of
728   water derived from wells". *Groundwater* 52, 100–111.
729 Kraijenhoff van de Leur, D. A. (1958). A study of non-steady ground-water flow with special
730   reference to the reservoir-coefficient, *De Ingenieur* 19, 87–94.
731 Lehner, B., Verdin, K. and Jarvis, A. (2008). New global hydrography derived from
732   spaceborne elevation data. *Eos* 89, 93–94.
733 Lehner, B., Ouellet Dallaire, C., Ariwi, J., Grill, G., Anand, M., Beames, P., Burchard-
734   Levine, V., Maxwell, S., Moidu, H., Tan, F. and Thieme, M. (2019). Global hydro-
735   environmental sub-basin and river reach characteristics at high spatial resolution. *Sci.*
736   *Data* 6, 283.
737 Lettenmaier, D. P., Alsdorf, D., Dozier, J., Huffman, G.J., Pan, M. and Wood, E.F. (2015).
738   Inroads of remote sensing into hydrologic science during the WRR era. *Water Resour.*
739   *Res.* 51, 7309–7342.
740 Linnansaari T, Monk, W.A., Baird, D.J. and Curry R. A. (2013*). Review of Approaches and*
741   *Methods to Assess Environmental Flows Across Canada and Internationally*. Canadian
742   Science Advisory Secretariat, Research Document 2012/039 (New Brunswick:
743   Department of Fisheries and Oceans Canada)
744 MacDonald, A., Bonsor, H., Ahmed, K. *et al.* (2016). Groundwater quality and depletion in
745   the Indo-Gangetic Basin mapped from *in situ* observations. *Nature Geosci.* **9,** 762–766.
746 MacEwan, D., Cayar, M., Taghavi, A., Mitchell, D., Hatchett, S. and Howitt, R. (2017).
747   Hydroeconomic modeling of stable groundwater management. *Water Resour. Res.* 53
748   2384–403
749 McCabe, M. F., Rodell, M., Alsdorf, D. E., Miralles, D. G., Uijlenhoet, R., Wagner, W.,
750   Lucieer, A., Houborg, R., Verhoest, N. E. C., Franz, T. E., Shi, J., Gao, H., and Wood, E.
751   F. (2017). The future of Earth observation in hydrology. *Hydrol. Earth Syst. Sci.* 21,
752   3879–3914.
753 McGuire, V.L. (2017). *Water-level changes in the High Plains aquifer, Republican River*
754   *Basin in Colorado, Kansas, and Nebraska, 2002 to 2015 (ver. 1.2, March 2017)*. U.S.
755   Geological Survey Scientific Investigations Map 3373, 10 p., 1 sheet with appendix,
756   https://doi.org/10.3133/sim3373.
757 Mukherjee, A., Bhanja, S.N. and Wada, Y. (2018). Groundwater depletion causing reduction
758   of baseflow triggering Ganges river summer drying. *Sci. Rep.* 8, 12049.
759 Pastor, A.V., Ludwig, F., Biemans, H., Hoff, H. and Kabat, P. (2014). Accounting for
760   environmental flow requirements in global water assessments. *Hydrol. Earth Syst. Sci.* 18
761   5041–59.
762 Perrone, D. and Jasechko, S. (2019). Deeper well drilling an unstable stopgap to groundwater
763   depletion. *Nat. Sustain.* 2**,** 773–782.

Richey, A. S., Thomas, B. F., Lo, M.-H., Reager, J.T., Famiglietti, J.S., Voss, K., Swenson, S. and Rodell, M. (2015). Quantifying renewable groundwater stress with GRACE. *Water Resour. Res*. 51, 5217–5238.

Runhaar ,H., Witte, J.P.M. and Verburg, P. (1997). Groundwater level, moisture supply, and vegetation in the Netherlands. *Wetlands* 17, 528–38.

Scanlon, B.R., Faunt, C.C., Longuevergne, L., Reedy, R.C., Alley, W.M., McGuire, V.L. and McMahon, P.B. (2012). Groundwater depletion and sustainability of irrigation in the U.S. High Plains and Central Valley. *P. Natl. Acad. Sci. U.S.A.* 109, 9320–9325.

Schellekens, J., Dutra, E., Martínez-de la Torre, A., Balsamo, G., van Dijk, A., Sperna Weiland, F., Minvielle, M., Calvet, J.-C., Decharme, B., Eisner, S., Fink, G., Flörke, M., Peßenteiner, S., van Beek, R., Polcher, J., Beck, H., Orth, R., Calton, B., Burke, S., Dorigo, W., and Weedon, G. P. (2017). A global water resources ensemble of hydrological models: the eartH2Observe Tier-1 dataset. *Earth Syst. Sci. Data* 9, 389–413.

Shafroth P.B., Stromberg J.C. and Patten D.T. (2000). Woody riparian vegetation response to different alluvial water table regimes Western North. *Am. Nat*. 60, 66–76.

Siebert, S., Kummu, M., Porkka, M., Döll, P., Ramankutty, N. and Scanlon, B.R. (2015). A global data set of the extent of irrigated land from 1900 to 2005. *Hydrol. Earth Syst. Sci* 19, 1521–1545.

Sutanudjaja, E. H., van Beek, R., Wanders, N., Wada, Y., Bosmans, J. H. C., Drost, N., van der Ent, R. J., de Graaf, I. E. M., Hoch, J. M., de Jong, K., Karssenberg, D., López López, P., Peßenteiner, S., Schmitz, O., Straatsma, M. W., Vannametee, E., Wisser, D., and Bierkens, M. F. P. (2018). PCR-GLOBWB 2: a 5 arcmin global hydrological and water resources model. *Geosci. Model Dev*. 11, 2429–2453.

Theis, C.V. (1940). The source of water derived from wells. *Civ. Eng*. 10, 277–280.

Bredehoeft, J.D. (2002). The water budget myth revisited: why hydrogeologists model. *Groundwater* 40, 340-345.

Wada, Y., van Beek, L.P.H. van Kempen, C.M., Reckman, J.W.T., Vasak, S., and Bierkens, M.F P. (2010). Global depletion of groundwater resources. *Geoph. Res. Lett.* 37, L20402.

Wada, Y., van Beek, L.P.H. and. Bierkens, M. F. P (2012). Nonstable groundwater sustaining irrigation: A global assessment, Water Resour. Res., 48, W00L06,

Wada Y., van Beek, L.P.H., Wanders and Bierkens M.F.P. (2013). Human water consumption intensifies hydrological drought worldwide. *Environ. Res. Lett*. 8, 034036.

Wada Y. (2016). Modeling Groundwater Depletion at Regional and Global Scales: Present State and Future Prospects. *Surv. Geophys.* 37, 419–451.

Watkins, M.M., Wiese, D.N., Yuan, D.-N., Boening, C., and Landerer, F.W. (2015). Improved methods for observing Earth's time variable mass distribution with GRACE using spherical cap mascons. *J. Geophys. Res.-Solid* 120, 2648–2671.

Wen, F. and Chen, X. (2006). Evaluation of the impact of groundwater irrigation on streamflow in Nebraska. *J. Hydrol.* 327, 603-617.

Wiese, D.N. (2015). GRACE monthly global water mass grids NETCDF RELEASE 5.0, Version 5.0, PO.DAAC, CA, USA, Dataset, available at: https://doi.org/10.5067/TEMSC-OCL05 (last access: 15 September 2017).

Wiese, D.N., Landerer, F.W., and Watkins, M.M. (2016). Quantifying and reducing leakage errors in the JPL RL05M GRACE mascon solution. *Water Resour. Res*. 52, 7490–7502.

808   Winter, T.C., Harvey, J.W., Franke, O.L. and Alley, W.A. (1998). *Ground water and surface*
809   *water: A single resource*. U.S. Geol. Surv. Circ., 1139.
810   Yin, L., Zhou, Y., Xu, D., Zhang, J., Wang, X., Ma, H. and Dong, J. (2018). Response of
811   phreatophytes to short-term groundwater withdrawal in a semiarid region: Field
812   experiments and numerical simulations *Ecohydrol.* 11, e1948.
813   Zipper, S.C., Dallemagne, T., Gleeson, T., Boerman, T.C., and Hartmann, A. (2018).
814   Groundwater pumping impacts on real stream networks: Testing the performance of
815   simple management tools. *Water Resourc. Res*. 54, 5471-5486.

Appendix A: Conceptual model for regional-scale groundwater pumping with groundwater-surface water interaction

A1. Basic equations

We repeat the three basic equations that make up the conceptual model regional-scale groundwater pumping with groundwater-surface water interaction:

The groundwater head as described with the total aquifer mass balance:

$$n\frac{dh}{dt} = r + F_{gw \leftrightarrow sw}(h) - q \tag{A1}$$

The groundwater - surface water flux:

$$F_{gw \leftrightarrow sw}(h) = \begin{cases} -\frac{h-h_s}{C} & h \geq d \\ \frac{h_s-d}{C} & h < d \end{cases} \tag{A2}$$

The surface water balance:

$$Q = Wv(h_s - d) = Q_i + q_sA - F_{gw \leftrightarrow sw}(h)A \tag{A3}$$

A2. The case $h(t) \geq d$ and $q < q_{crit}$

We will start by analyzing the case that $h \geq d$, i.e. the groundwater level is attached to the surface water body. We further assume that $q < q_{crit}$, i.e. the groundwater withdrawal is such that the groundwater level never falls below the surface water bottom level d. In this case, the surface water flux Q (m³/day) is related to the groundwater and surface water level as follows (See Figure A1):

$$Q = Wv(h_s - d) = Q_i + q_sA + \frac{h-h_s}{C}A \tag{A3}$$

with

A: The area over (sub-)aquifer considered (m²)

q_s: surface runoff (m d⁻¹)

Q_i: influx of surface water from upstream (m³ d⁻¹)

W: Stream width (m)

d: Bottom elevation stream (m)

v: Stream flow velocity (m d⁻¹)

$$Q = Q_i + (q_s - F_{gw \leftrightarrow sw}) \cdot A = W \cdot v \cdot (h_s - d)$$

844
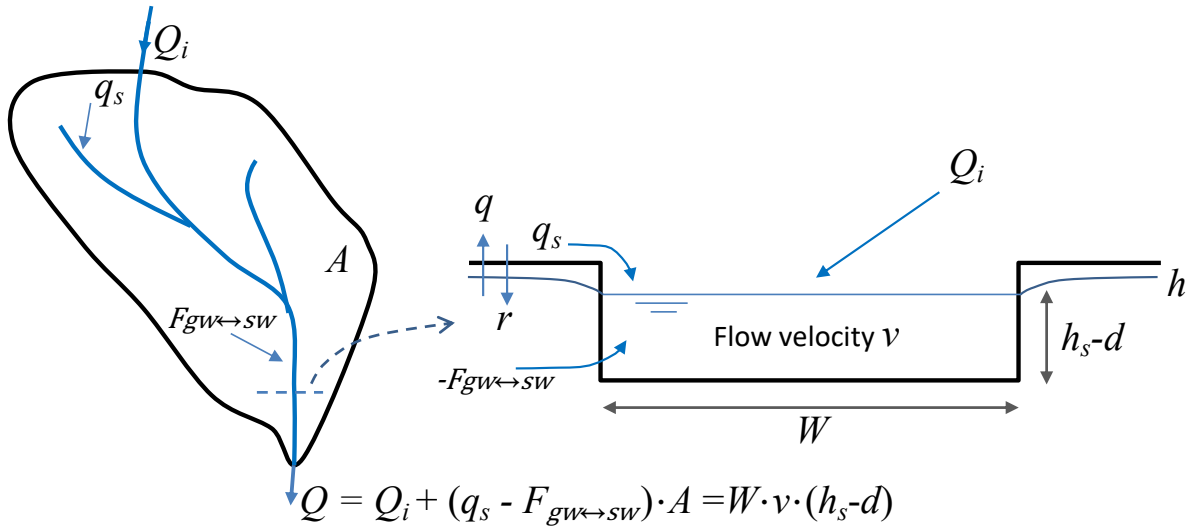
845   *Figure A1. Contributing fluxes to streamflow.*

846

847   Collecting h_s on one side and the other terms on right side results in the following relation

848   between surface water height and groundwater head:

849    $\quad\quad h_s(t) = \alpha + \beta h(t)$ $\hfill$ (A4)

850   with

851    $\quad\quad \alpha = \dfrac{Q_i C + q_s A C + W v d C}{W v C + A}$ $\hfill$ (A5)

852    $\quad\quad \beta = \dfrac{A}{W v C + A}$ $\hfill$ (A6)

853   From (A1) and (A2) the differential equation for groundwater level gives:

854    $\quad\quad n\dfrac{dh}{dt} = r - \dfrac{h - h_s}{C} - q$ $\hfill$ (A7)

855   And after substituting (A4)

856    $\quad\quad \Rightarrow n\dfrac{dh}{dt} = \left(r + \dfrac{\alpha}{C} - q\right) - \left(\dfrac{1 - \beta}{C}\right)h$ $\hfill$ (A8)

857   From (A8) follows the steady-state groundwater level under natural conditions ($q = 0$ and

858    $dh/dt = 0$):

859    $\quad\quad \bar{h}_{nat} = \dfrac{rC + \alpha}{1 - \beta}$ $\hfill$ (A9)

860   Solving differential equation (A8) for initial condition (A9) then yields:

861    $\quad\quad h(t) = \dfrac{rC + \alpha}{1 - \beta} - \left(\dfrac{qC}{1 - \beta}\right)\left[1 - e^{-\left(\frac{1 - \beta}{nC}\right)t}\right]$ $\hfill$ (A10)

862   Which also gives the equilibrium groundwater level for $t \rightarrow \infty$:

863    $\quad\quad h(\infty) = \dfrac{rC + \alpha - qC}{1 - \beta}$ $\hfill$ (A11)

864   The surface water level with time is given by (A4) and the final equilibrium surface water

865   follows from (A4) and (A11) as:

866 $$h_s(\infty) = \alpha + \frac{\beta(rc + \alpha - qC)}{1 - \beta} \quad (A12)$$

867 The surface water discharge as a function of time follows from combining (A3) and (A4):

868 $$Q(t) = Q_i + q_s A - \frac{A\alpha}{C} + \frac{A(1-\beta)}{C} h(t) \quad (A13)$$

869 with $h(t)$ given by (A10). The equilibrium discharge is obtained by substituting (A11) for

870 $h(\infty)$ in (A13):

871 $$Q(\infty) = Q_i + (q_s + r - q)A \quad (A14)$$

872 Which also follows logically from the water balance.

873

874 **A3. The critical withdrawal rate q_{crit}**

875 The critical withdrawal rate determines whether at larger times the water table drops below

876 the bottom of the surface and moves to the physically unstable regime. We seek q such that

877 $h(\infty) = d$:

878 $$\frac{rC + \alpha - qC}{1 - \beta} = d \quad (A15)$$

879 From which follows:

880 $$q = \frac{rC + \alpha - d(1 - \beta)}{C} \quad (A16)$$

881 Substituting α and β yields after some manipulation:

882 $$q_{\text{crit}} = r + \frac{Q_i + q_s A}{WvC + A} \quad (A17)$$

883

884 **A4. Critical transition time t_{crit} in case $q > q_{\text{crit}}$**

885 In case $q > q_{\text{crit}}$ at some time after pumping (t_{crit}) the groundwater level will fall below the

886 bottom elevation d of the surface water. Before that time, it follows the water table decline

887 according to (A10). So, we can find t_{crit} by solving it from:

888 $$h(t_{\text{crit}}) = \frac{rC + \alpha}{1 - \beta} - \left(\frac{qC}{1-\beta}\right)\left[1 - e^{-\left(\frac{1-\beta}{nC}\right)t_{\text{crit}}}\right] = d \quad (A18)$$

889 Solving an equation of the form $a - b[1 - e^{-c\,x}] = d$ gives as solution: $x = \frac{1}{c}\ln\left(\frac{b}{d - a + b}\right)$

890 from which follows from (A18):

891 $$t_{\text{crit}} = \frac{nC}{1 - \beta}\ln\left(\frac{qC}{qC - (rC + \alpha) + d(1 - \beta)}\right) \quad (A19)$$

892

893 **A5. The case $q > q_{\text{crit}}$ and $t > t_{\text{crit}}$ ($h(t) < d$)**

894 In case the water table is below the bottom elevation of the stream, the water balance of the

895 stream reads (see Fig. A2):

896 $$Q = Wv(h_s - d) = Q_i + q_s A - \frac{h_s - d}{C} A \qquad (A20)$$

897 From which we can derive an equation for the minimum and constant elevation of the surface

898 water level (valid for $t > t_{\text{crit}}$):

899 $$h_s = d + \frac{(Q_i + q_s A)C}{WvC + A} \qquad (A21)$$

900
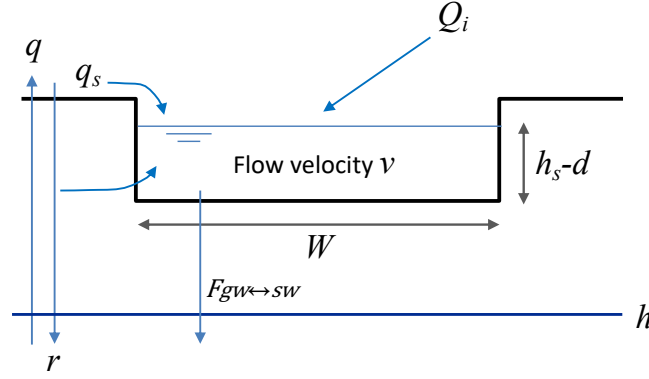
901 *Figure A2. Water balance of a stream in case $q > q_{crit}$ and $t > t_{crit}$ $(h(t) < d)$*

902

903 The differential equation describing the change in groundwater with time now becomes:

904 $$n \frac{dh}{dt} = r - q + \frac{h_s - d}{C} \qquad (A22)$$

905 Substituting $h_s - d$ from (A21) then yields an equation for the groundwater decline rate:

906 $$\frac{dh}{dt} = \frac{r - q}{n} + \frac{(Q_i + q_s A)}{n(WvC + A)} \qquad (A23)$$

907 which is always negative since $q > q_{\text{crit}}$. With initial condition $h(t_{\text{crit}}) = d$ one obtains from

908 (A23) and equation for $h(t), t > t_{\text{crit}}$:

909 $$h(t) = d + \left[\frac{r - q}{n} + \frac{(Q_i + q_s A)}{n(WvC + A)} \right] (t - t_{\text{crit}}) \qquad (A24)$$

910

911 **A5. Sources of pumped groundwater: $q < q_{crit}$ or $t < t_{crit}$ $(h(t) \geq d)$**

912 When neglecting direct evaporation from groundwater, the sources of pumped groundwater

913 in case $q < q_{crit}$ either come out of storage or from recharge that does not contribute to

914 streamflow. The latter is called "capture". From the water balance (A1) we thus find:

915 $$q = r + F_{gw \leftrightarrow sw}(h(t)) - n \frac{dh}{dt} \qquad (A25)$$

916 The first two terms constitute the water pumped from capture (with $F_{gw \leftrightarrow sw}$ negative in case

917 $h > h_s$ and positive when $h < h_s$) and the second term the water out of storage. Furthermore,

918 from differentiation of (A10) we have:

919 $$n\frac{dh}{dt} = -qe^{-\left(\frac{1-\beta}{nC}\right)t}$$ (A26)

920 Combining (A26) and (A25) then gives (since capture + out of storage add up to q):

921

922 $$q = \underbrace{q\left(1 - e^{-\left(\frac{1-\beta}{nC}\right)t}\right)}_{r + F_{gw \leftrightarrow sw}} + \underbrace{qe^{-\left(\frac{1-\beta}{nC}\right)t}}_{-n\frac{dh}{dt}}$$ (A27)

923

924

925 This shows that the fraction groundwater taken out of storage reduces over time until head

926 decline stops and all water comes out of capture.

927

928 **A6. Sources of pumped groundwater: $q > q_{crit}$ and $t > t_{crit}$ ($h(t) < d$)**

929 In case $q > q_{crit}$ and $t < t_{crit}$ the sources of pumped groundwater follow (A27). After the

930 groundwater table falls below the bottom elevation of the stream and $t > t_{crit}$ the sources of

931 water follow from (A23):

932 $$n\frac{dh}{dt} = r - q + \frac{(Q_i + q_s A)}{(WvC + A)}$$ (A28)

933 And therefore:

934 $$q = r + \frac{(Q_i + q_s A)}{(WvC + A)} - n\frac{dh}{dt}$$ (A29)

935 Since the third term is the storage change and capture plus storage change add up to q we

936 have:

937 $$q = \underbrace{r + \frac{(Q_i + q_s A)}{(WvC + A)}}_{r + F_{gw \leftrightarrow sw}} + \underbrace{q - \left(r + \frac{(Q_i + q_s A)}{(WvC + A)}\right)}_{-n\frac{dh}{dt}}$$ (A30)

938

939

940 which shows that at after $t > t_{crit}$ the ratio of pumping from capture (i.e. recharge and surface

941 water leakage) and storage change becomes constant.

942

943

Appendix B: Relationship between groundwater response time J and drainage resistance C

In PCR-GLOBWB 2 (Sutanudjaja et al., 2018) and in similar global hydrological models, the relationship between groundwater discharge Q_g (m^3 m^{-2} d^{-1}) and the volume V_g (m^3/m^2) stored in the groundwater store is given by a simple linear relationship:

$$Q_g = \frac{V_g}{J} \tag{B1}$$

With J the characteristic response time of the groundwater system (e-folding time of the recession) (days). In some of the global models J is obtained by calibration to low flows or recession curves. In PCR-GLOBWB it is calculated from transient drainage theory of Kraijenhoff-van de Leur (1958) as:

$$J = \frac{nL^2}{\pi^2 T} \tag{B2}$$

with n the drainable porosity or specific yield, L the average distance between water courses (derived from the drainage density per cell) and T the aquifer transmissivity obtained from global hydrogeological datasets (e.g. Gleeson et al., 2014). A similar approach was used by Cuthbert et al. (2019) to derive groundwater response times.

The drainable volume of groundwater stored in the groundwater reservoir (m^3 m^{-2}) of a grid cell of a global hydrological model can also be expressed as: $V_g = n(h - h_s)$, with h_s the surface water level and h the groundwater level in the cell. Substituting this into (B1) we obtain the equivalent groundwater drainage equation for a grid cell:

$$Q_g = \frac{n(h - h_s).}{J} \tag{B3}$$

Comparing (B3) with (A2) shows that to obtain the same groundwater-surface water exchange in the global hydrological model and the conceptual analytical model we must have:

$$C = \frac{J}{n} \tag{B4}$$

Note that these relationships assume that the streams remain connected with the surface water, which is not entirely consistent with Equation A2.